JACS
JOURNAL OF THE AMERICAN CHEMICAL SOCIETY
Article
pubs.acs.org/JACS

Substituent Effects on the Electronic Characteristics of Pentacene Derivatives for Organic Electronic Devices: Dioxolane-Substituted Pentacene Derivatives with Triisopropylsilylethynyl Functional Groups

Olga Lobanova Griffith,*[,†] John E. Anthony,*[,‡] Adolphus G. Jones,[‡] Ying Shu,[‡] and Dennis L. Lichtenberger*[,†]

[†]Department of Chemistry and Biochemistry, The University of Arizona, Tucson, Arizona 85721-0041, United States
[‡]Department of Chemistry, University of Kentucky, Lexington, Kentucky 40506-0055, United States

Supporting Information

ABSTRACT: The intramolecular electronic structures and intermolecular electronic interactions of 6,13-bis-(triisopropylsilylethynyl)pentacene (TIPS pentacene), 6,14-bis-(triisopropylsilylethynyl)-1,3,9,11-tetraoxa-dicyclopenta[*b*,*m*]-pentacene (TP-5 pentacene), and 2,2,10,10-tetraethyl-6,14-bis-(triisopropylsilylethynyl)-1,3,9,11-tetraoxa-dicyclopenta[*b*,*m*]-pentacene (EtTP-5 pentacene) have been investigated by the combination of gas-phase and solid-phase photoelectron spectroscopy measurements. Further insight has been provided by electrochemical measurements in solution, and the principles that emerge are supported by electronic structure calculations. The measurements show that the energies of electron transfer such as the reorganization energies, ionization energies, charge-injection barriers, polarization energies, and HOMO−LUMO energy gaps are strongly dependent on the particular functionalization of the pentacene core. The ionization energy trends as a function of the substitution observed for molecules in the gas phase are not reproduced in measurements of the molecules in the condensed phase due to polarization effects in the solid. The electronic behavior of these materials is impacted less by the direct substituent electronic effects on the individual molecules than by the indirect consequences of substituent effects on the intermolecular interactions. The ionization energies as a function of film thickness give information on the relative electrical conductivity of the films, and all three molecules show different material behavior. The stronger intermolecular interactions in TP-5 pentacene films lead to better charge transfer properties versus those in TIPS pentacene films, and EtTP-5 pentacene films have very weak intermolecular interactions and the poorest charge transfer properties of these molecules.

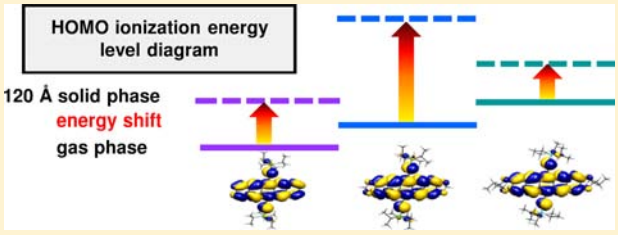

1. INTRODUCTION

Pentacene derivatives have attracted attention due to their applications as the electroactive part of organic field effect transistors (OFETs), organic photovoltaics (OPV), and organic light emitting diodes (OLEDs).[1−15] The diversity of applications of pentacenes is possible because the electronic and optical properties of these materials are tunable for a particular device by adding different functional groups to the pentacene backbone. For example, the addition of the triisopropylsilylethynyl groups to the 6 and 13 positions of pentacene leads to a soluble and stable 6,13-bis-(triisopropylsilylethynyl) (TIPS) pentacene compound **1** (see Chart 1) which adopts a 2D π-stacking arrangement in the solid, thus making TIPS pentacene suitable for OFETs.[15−19] Further functionalization of TIPS pentacene by dioxolane substituents added to the terminal fused rings leads to the highly fluorescent 6,14-bis-(triisopropylsilylethynyl)-1,3,9,11-tetraoxa-dicyclopenta[*b*,*m*]-pentacene (TP-5 pentacene, **2**), and 2,2,10,10-tetraethyl-6,14-bis-(triisopropylsilylethynyl)-1,3,9,11-tetraoxa-dicyclopenta[*b*,*m*]pentacene (EtTP-5 pentacene, **3**), which can be used in OLEDs.[10,18] TP-5 pentacene **2** adopts a 1D π-stacking arrangement with significant π-orbital overlap in the solid, thus becoming also suitable for OFETs.[18,20] EtTP-5 pentacene **3** has a large separation between π-faces in the crystal due to the ethyl groups on the dioxolane rings, which hinders the interaction between pentacene units in the solid.[18,21] All three pentacene derivatives (TIPS, TP-5, and EtTP-5) have also been used in OPVs as electron donors.[1]

In this work, energy measurements of molecular electronic structures and properties (such as ionization energies, reorganization energies, charge-injection barriers, HOMO/LUMO energy gaps, and polarization energies) of TIPS, TP-5, and EtTP-5 pentacenes and how these electronic properties are altered in the condensed phases are reported on the basis of gas- and solid-phase photoelectron spectroscopy, along with

Received: June 11, 2012
Published: August 6, 2012

dx.doi.org/10.1021/ja3056672 | J. Am. Chem. Soc. 2012, 134, 14185−14194

Chart 1. TIPS Pentacene, 1, TP-5 Pentacene, 2, and EtTP-5 Pentacene, 3

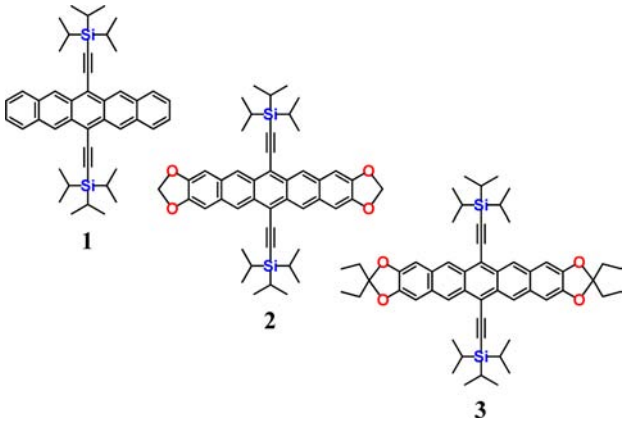

electrochemistry experiments. The experimental results are further supported by quantum-mechanical calculations at the density functional theory level. The main focus of this study is to understand how the electronic properties and polarization effects of TIPS-substituted pentacenes are affected by substitutions of the pentacene core with dioxolane-containing groups at the terminal positions in all three phases: gas, solution, and solid. From the gas-phase analysis, the values of the vertical and adiabatic ionization energies, as well as the intramolecular reorganization energies are obtained; solution phase study provides the oxidation and reduction potentials and correspondingly derived HOMO/LUMO energy gaps. The solid-phase analysis gives the ionization and polarization energies, along with charge-injection barriers in the presence of intermolecular interactions.

2. EXPERIMENTAL AND COMPUTATIONAL DETAILS

2.1. Gas-Phase Photoelectron Spectroscopy. Gas-phase photoelectron spectra (He I photon source) were recorded on an instrument built around a 360 mm radius, 80 mm gap hemispherical analyzer[22] (McPherson) using a custom-designed photon source and gas-phase sample cell.[23,24] Instrument control and electron counting are interfaced to a National Instruments PCIe-6259 multifunction DAQ board and custom software. Samples sublimed cleanly with no evidence of decomposition. Sublimation temperatures as monitored with a K-type thermocouple passed through a vacuum feed and attached directly to the ionization cell were 285−300 °C for **1**, 265−302 °C for **2**, and 255−265 °C for **3**. The argon $^2P_{3/2}$ ionization at 15.759 eV was used as an internal calibration lock of the absolute ionization energy and its difference with the CH_3I $^2E_{1/2}$ ionization at 9.538 eV provided an external calibration of the energy scale. The instrument resolution (measured as the full width at half-maximum (fwhm) of the argon $^2P_{3/2}$ ionization) was 0.026−0.027 eV during data collection. The intensity of the ionizations was corrected according to an experimentally determined analyzer sensitivity function versus electron kinetic energy. The He I spectra were also corrected for the He Iβ resonance line emission from the source, which is about 3% of the intensity of the He Iα line emission and at 1.869 eV higher photon energy.

2.2. Solid-Phase Photoelectron Spectroscopy. The photoelectron spectra of thin films (prepared as described below) of **1**−**3** were collected at room temperature using a combined UPS-XPS Kratos Axis Ultra instrument with an average base pressure at or below 5×10^{-8} Torr, and the analyzer was operated in the constant analyzer energy (CAE) mode. UPS (valence) studies were performed using a gas discharge lamp (Omicron VUV Lamp HIS 13) producing He I (He Iα; 21.218 eV) photons, and the spectra were collected using a 5 eV pass energy. An accelerating bias voltage of 9 V was applied during the UPS data collection to improve the transmission of electrons with very low kinetic energy. XPS (core) studies were performed using a monochromatic Al Kα (1489 eV) excitation source, with pass energies of 20 eV for close-up spectra of the O 1s, C 1s, and Si 2p ionizations for **1**−**3**. The HBEC (high binding energy cutoff of electron counts) of solid-phase UPS spectra was taken as the highest binding energy point at which electron counts are above the baseline (and was obtained as the cross point of the tangent to the high binding energy side with the baseline. The adiabatic ionization energy was determined similarly as the onset of electron counts above the baseline on the low binding energy side of the spectra (which was determined as the cross point of the tangent to the low energy side of the first ionization energy band with the baseline). The uncertainty in these energies is generally about ±0.1 eV and may be more when the signal is broadened, such as for the first ionization of molecule **3** at higher coverages. The instrument kinetic energy scale was calibrated for UPS measurements using the He I and He II energy sources, such that the kinetic energy difference of Au 5d ionizations measured by UPS in He II and He I modes is equal to the energy difference between He II and He I energy sources, 40.8 eV − 21.2 eV = 19.6 eV.

2.2.1. Thin-Film Preparation. The films of substituted pentacenes **1**−**3** were prepared by vapor deposition on a gold foil substrate in a UHV chamber connected to the UPS/XPS analysis chamber. We focus on the electronic properties of the films directly as deposited. Surface contaminants were removed from the gold foil prior to use by sputtering the surface with an argon ion beam set to 10−15 mA. The solid oligoacene samples were placed into a boron nitride crucible and sublimed under vacuum (at or below 5×10^{-6} Torr) using a stainless steel Knudsen cell. A tantalum sleeve was attached to the top of the cell to help direct the sublimed sample for deposition on the gold substrate. Sublimation temperatures were monitored using a K-type thermocouple passed through an ultrahigh vacuum (UHV) feed and attached directly to the sample cell. Successive depositions were made at 275−295 °C for **1**, 250−260 °C for **2**, and 230−240 °C for **3**. Film thicknesses were determined by monitoring the change in frequency of a quartz crystal microbalance (QCM) mounted parallel to the gold substrate in the deposition chamber. A change in frequency of 15 Hz was determined to correspond to approximately 3 Å of each sample (roughly a monolayer thickness), as also confirmed by attenuation of the Au $3d_{5/2}$ signal in the XPS spectrum. Subsequent depositions of molecules **1**−**3** on Au were made in multiple steps with thicknesses from 10 to 200 Å for TIPS pentacene and TP-5 pentacene, and from 6 to 120 Å for EtTP-5 pentacene. The deposition rate was 1 Hz per 1 s for all molecules. After each deposition of the sample, the UPS spectra were collected followed by the collection of XPS spectra. There was no evidence of decomposition of the films over the course of these measurements.

2.3. Electrochemistry. Electrochemical data were measured using a BAS CV-50W voltammetric analyzer in a three cell configuration consisting of a Ag wire pseudo reference electrode, a platinum button as working electrode and a platinum wire as counter electrode. Tetrabutylammonium hexafluorophosphate ($TBAPF_6$) was dissolved in dichloromethane (DCM) to produce 0.1 M supporting electrolyte solution. Both cyclic voltammetry (CV) and differential pulse voltammetry (DPV) were performed for each acene. The system was calibrated versus the ferrocene/ferrocenium redox couple. The optimal potential window for all compounds was determined using CV, then the anodic and cathodic electrochemical processes were studied individually using DPV. Redox potentials were obtained from DPV experiments. For CV we use a scan rate of 50 mV/s and for DPV 20 mV/s. These voltammetry measurements were then converted to absolute electrochemical HOMO−LUMO values and band gaps using the absolute HOMO energy of ferrocene of 4.8 eV according to literature methods.[25,26] The uncertainty of electrochemical measurements is approximately ±0.05 V.

2.4. Computations. Computations were performed with the Gaussian 03[27] and ADF2008[28] programs using several density functionals and basis sets (see Supporting Information for additional details). Because a large number of different conformations are possible for the TIPS groups on the pentacenes, starting structures for

dx.doi.org/10.1021/ja3056672 | J. Am. Chem. Soc. 2012, 134, 14185−14194

the geometry optimizations were selected in two different ways. In the first approach, the starting coordinates were taken from the crystal structure of TIPS pentacene.[17] In the second approach, the possible gas phase conformations of TIPS pentacene were generated with MacroModel,[29] and the starting coordinates were taken from the lowest energy conformation. Optimization of the geometries from both sets of starting coordinates led to the same structures and energies, which implies that crystal packing in the solid state does not change the preferred conformation of the TIPS groups. The substituents of the TP-5 pentacene **2** and EtTP-5 pentacene **3** molecules were then added to the TIPS pentacene core structure and the full structures were optimized in the gas phase.

The B3LYP energy functional has been applied extensively to calculations of the electronic properties of organic molecules,[7,30−32] and we reported earlier that ΔSCF calculations for TIPS-substituted oligoacenes using the B3LYP/6-31G** model reproduce the gas phase experimental trends.[33] Here we use the geometries optimized at the B3LYP/6-31G** level. The calculated gas-phase ionization energies are smaller than the corresponding experimental values by about 0.6 eV for pentacenes **1**−**3** by this model, and the reorganization energies are underestimated by about 50 meV, but the computational energy trends reproduce the experimental trends in the gas phase correctly. The calculated ionization energies come closer to the experimental values with the M06 functional and especially with triple-ζ functions such as cc-pTVZ and TZVP. The M06/TZVP energies at the B3LYP/6-31G** geometries consistently underestimate the ionization energies and absolute oxidation and reduction potentials by about 0.3 eV. Geometry optimizations at the M06/TZVP level were prohibitively time-consuming for this study.

3. RESULTS AND DISCUSSION

The main goal of this work is to analyze the electronic properties of the valence states of TIPS pentacenes **1**−**3** in the gas, solution, and solid phases with emphasis on the electronic effects of the dioxolane substituents on the TIPS pentacene core.

3.1. Gas Phase. The molecular vertical and adiabatic ionization energies along with the intramolecular reorganization energies of TIPS, TP-5, and EtTP-5 pentacenes are obtained from the gas-phase ultraviolet photoelectron spectroscopy (UPS) measurements of the first ionization bands, shown in Figure 1. The full spectra for these molecules are given in the Supporting Information. Before proceeding to a detailed analysis of the first ionization bands, first consider the information that is readily apparent from visual comparison of the ionizations. From Figure 1 one can see that the position and width of the first ionization energy band strongly depends on the particular substitution of the pentacene backbone at the terminal positions. A first approximation to the vertical ionization energy (VIE) is simply the energy of the most intense feature in the ionization band, because this feature represents the transition from the most probable geometry in the ground vibrational state of the neutral molecule to the (vertical) vibrational state of the cation with minimal change in geometry. The adiabatic ionization energy (AIE) is approximated by the low energy onset of the ionization band, corresponding to the transition from the ground state of the neutral molecule to the ground state of the cation upon ionization, provided that the reorganization energy is sufficiently small relative to the vibrational displacements of the neutral molecule and that hot bands do not obscure the adiabatic onset (vide infra). The intramolecular reorganization energy (RE) is the energy difference from the VIE to the AIE, and larger reorganization energies are evidenced by larger ionization band widths. As seen in Figure 1, the first ionization band shifts to lower ionization energy and becomes broader

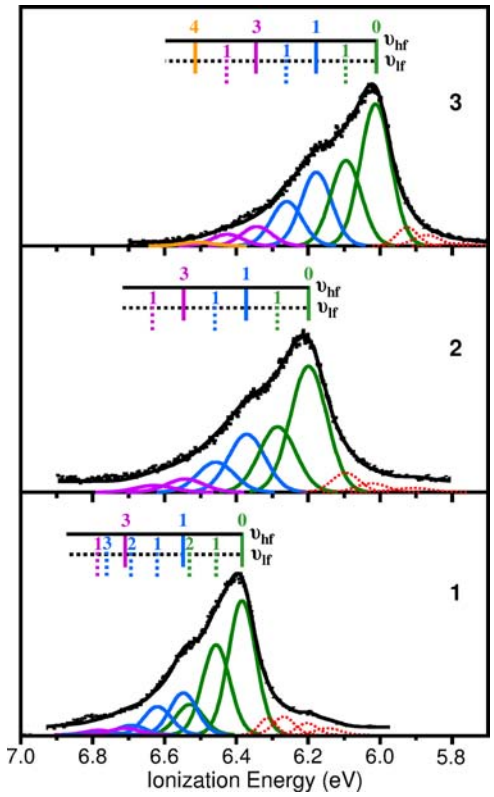

Figure 1. He I gas-phase UPS: first ionization energy bands of molecules **1**−**3**.

going from TIPS pentacene **1** to TP-5 pentacene **2**, and further to EtTP-5 pentacene **3**, reflecting decreasing vertical and adiabatic ionization energies and increasing reorganization energies on going from molecule **1** to molecule **3**.

More precise values of the vertical ionization energies (VIE) and the radical cation reorganization energies (RE) of molecules **1**−**3** were obtained from analytical evaluation of the ionization band contours. This analysis is based on the two-mode Poisson vibrational progression model, which was successfully applied earlier to analysis of the ionization energies and reorganization energies of other TIPS oligoacenes, including TIPS pentacene,[33] and has been discussed in detail previously in several earlier reports.[32,34−36] Briefly, the high frequency vibrations activated upon ionization are modeled by vibrational components constrained to Poisson intensity distributions, and the width of the high frequency vibrational components is determined by the instrumental peak broadening and unresolved low-frequency vibrations that give a Gaussian peak shape. The Poisson vibrational distributions that model the ionization energy bands for each molecule are represented as color coded peaks under each band in Figure 1. Although the model shown in Figure 1 has many vibrational peaks contributing to the overall shape, there are actually few variable parameters in modeling the data. After the Gaussian line shape is determined and held the same for all components, only the vibrational spacing and Huang−Rhys factor of each progression are optimized to match the band contour.

Because of the high sublimation temperature of pentacenes **1**−**3** (265−315 °C), the low-lying vibrationally excited levels in the ground state of these molecules were thermally populated, which in turn resulted in the presence of the so-called hot bands[33,34] on the low energy side of the first ionization band.

dx.doi.org/10.1021/ja3056672 | J. Am. Chem. Soc. 2012, 134, 14185−14194

These hot bands are shown in Figure 1 by the red dashed lines, and their presence was taken into account when determining the VIE, AIE, and RE, but did not affect these ionization and reorganization energy values.

According to this vibrational analysis,[33] the RE consists of two contributions: quantum-mechanical and semiclassical. The quantum-mechanical portion of the RE takes into account the Poisson intensity distribution in each vibrational progression (defined by the Huang–Rhys factor) and the energy separation between peaks (that is, the vibrational frequency of the progression). The uncertainty in the determination of RE turns out to be less than the individual uncertainties in the vibrational frequency and the Huang–Rhys factor, because the RE is a function of the product of the two, and in the modeling of ionization intensity an overestimate of the vibrational frequency is accompanied by an underestimate of the Huang–Rhys factor. The semiclassical part of the RE takes into account the width of the Gaussians within each progression (after allowance for the instrumental broadening) and the sublimation temperature of each sample. The adiabatic ionization energy (AIE) is then determined as the difference between the vertical ionization energy and the intramolecular reorganization energy rather than trying to observe the ionization to the ground vibrational state of the radical cation. Previous theoretical studies of pentacene have shown that the overall ionization band contour is a complex manifold of overlapping vibrational progressions,[37] but the reorganization energy obtained from the multimode analysis is the same as obtained from the two-mode analysis, which essentially integrates the multimode intensity. The addition of more vibrational progressions did not improve the fit of the energy band and did not affect the energy values obtained from this two-mode fit.

The main energy parameters obtained from this two-mode fit are presented in Table 1. The uncertainties in the reported energies are on the order of ±0.005 eV. The detailed information about the vibrational analysis with the complete list of parameters for each molecule is given in the Supporting Information. The higher frequency vibrational progression (ν_{hf}) describes vibrations of about 1300–1400 cm^{-1} originating mainly from the vibrations of the pentacene core activated upon ionization, whereas the lower frequency progression (ν_{lf}) corresponds to the vibrations of about 600–700 cm^{-1} caused primarily by the vibrations of the TIPS groups for all three molecules. Qualitatively, the observed shoulder on the high energy side of the first ionization band for each molecule signifies the presence of the high frequency vibrational mode, and the high energy skew of the band reflects the presence of the low frequency mode.

Table 1. Energy Values from Two-Mode Modeling of the First Ionization Bands[a]

molecule	ν_{hf}, cm^{-1}	ν_{lf}, cm^{-1}	RE, meV	VIE, eV	AIE, eV
1	1338	622	111	6.39	6.28
2	1383	694	135	6.20	6.06
3	1333	665	141	6.01	5.87

[a]Full set of parameters for each two-mode Poisson analysis of the band profiles is given in Supporting Information. ν_{hf} and ν_{lf} are the high and low frequency vibrational modes respectively; RE is the reorganization energy; VIE and AIE are the vertical and adiabatic ionization energies respectively.

On the basis of both visual inspection of the ionizations and more precise analysis, the addition of dioxolane substituents leads to lower ionization energy in the gas phase and larger reorganization energy for TIPS pentacenes. Even though the oxygen atoms are more electronegative than carbon atoms (what causes stabilization of the HOMO energy levels by an inductive effect), the pi conjugation increases upon dioxolane substitution of the acene core and causes the destabilization of the HOMO by an overlap effect, thus opposing and dominating over the electronegativity effect. This effect of dioxolane groups was also observed for benzene and naphthalene: the VIE change on going from benzene (9.24 eV)[38] to 1,3-benzodioxole (8.18 eV)[39,40] is 1.06 eV and from naphthalene (8.15 eV)[38] to 2,3-(methylenedioxy)naphthalene (7.88 eV)[40,41] is 0.27 eV; and for the sake of comparison, in this work the VIE shift on going from TIPS pentacene to TP-5 pentacene is 0.19 eV. The dioxolane substitutions of TIPS pentacene contribute toward the high vibrational frequency mode due to increased pi conjugation on going from molecule **1** to **3**, thus leading to larger reorganization energy.

3.2. Solution Phase. The solution oxidation and reduction electronic properties of pentacenes **1**–**3** are evaluated electrochemically. Comparison of the solution-phase oxidation potentials with the gas-phase ionization energies provides a better understanding of the change in the electronic properties of these pentacenes going from the gas to the condensed phase, taking into account the differences between the electrochemical free energy measure in solution and the photoelectron spectroscopic energy measure in the gas phase (see Section 3.3).[42−46] According to the electrochemical measurements in dichloromethane solution with respect to Fc/Fc^+, the oxidation potential of TIPS pentacene **1** is 0.37 V, of TP-5 pentacene **2** is 0.24 V, and that of EtTP-5 pentacene **3** is 0.18 V; the reduction potentials are −1.47, −1.55, and −1.66 V for molecules **1**, **2**, and **3**, respectively. The decreasing oxidation potentials and more negative reduction potentials through the series reflect the same trend of decreasing gas-phase ionization energies. The correlation between the solution-phase oxidation potentials and the gas-phase ionization energies, with a slope of 0.47, is shown in Figure 2. The slope of this correlation is noticeably less than unity meaning that the solvent effects on these pentacenes cause an attenuated change in oxidation potentials versus the change in ionization energies for molecules **1**–**3**, but the

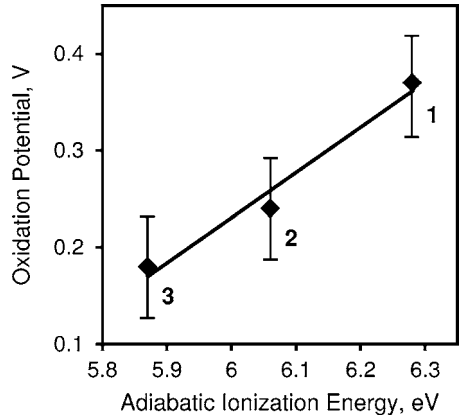

Figure 2. Correlation between the experimental oxidation potentials (vs Fc/Fc^+) and the gas-phase adiabatic ionization energies for molecules **1**–**3**.

dx.doi.org/10.1021/ja3056672 | J. Am. Chem. Soc. 2012, 134, 14185–14194

solvent effects are not strong enough to drastically change the oxidation potential trend from the ionization energy trend.

The absolute values of the HOMO and LUMO energy levels are obtained according to the common literature method[25,26] (see Experimental and Computational Details section) of adjusting the measured oxidation and reduction potentials to the absolute reference potential. These values along with the energy gap in dichloromethane solution are reported in Table 2. As can be seen from Table 2, the shifts in HOMO and LUMO energy levels between molecules **1**–**3** are in the same direction by about the same amount, such that these pentacenes have the same (within experimental error) energy gap values.

Table 2. Absolute Energy Levels in eV of Molecules 1–3 Based on Adjusted Experimental Oxidation and Reduction Potentials[a]

molecule	HOMO	LUMO	Gap
1	−5.16	−3.33	1.83
2	−5.04	−3.26	1.78
3	−4.98	−3.14	1.84

[a]Measured in dichloromethane and adjusted as explained in the Experimental and Computational Details section.

3.3. Computations. Two caveats should be kept in mind when discussing the HOMO and LUMO energy levels and the energy band gap. First, the precise meaning of the reported energy values depends on the experimental method by which they are measured and the theory by which they are interpreted. In this case, the experimental definition of the HOMO and LUMO energy levels based on absolute oxidation and reduction potentials is not the same as the precisely defined HOMO and LUMO orbital energies in Hartree–Fock theory. However, these two definitions (as well as other experimental measures and theoretical definitions of the HOMO and LUMO energies) share the concept of electronic states related by loss and gain of electrons and often trend similarly. The energies are directly linked as shown computationally in this section. Second and most important to the results of this study, the discussion in terms of HOMO and LUMO energy levels can be misleading because it implies that these energy levels are intrinsic properties of the neutral molecules that control the energies of electron transfer. As will be shown in Section 3.4, consideration must be given to the particular nature of the cation and anion electronic states rather than the electronic structure of the neutral molecules, and the influence of the molecular environment on these ionic electronic states.

The trends in the measured gas-phase photoelectron ionization energies and solution electrochemical oxidation and reduction potentials are compared to the electronic structure computations at the DFT level in Figure 3. The gas-phase ionization energies are calculated as the ΔE_{SCF} electronic energy from the neutral molecule to the cation at the neutral molecule optimized geometry (VIE) and to the cation at cation optimized geometry (AIE). The VIE contains the electron relaxation energy and change in correlation energy according to the DFT model, and the AIE adds the reorganization energy.

Calculation of the free energies (ΔG) of the solution oxidation and reduction potentials starts from the gas-phase adiabatic ionizations energies and electron affinities respectively and proceeds to inclusion of the changes in thermal and solvation free energies with removal and addition of an electron to the molecule. It was anticipated that changes in zero-point energies and thermal free energies would be small because the reorganization energies are relatively small and there is relatively little change in the vibrational energies and shapes of the molecules. As a check of this expectation, the vibrational frequencies of the neutral and cation states of pentacene and TIPS pentacene were calculated and the gas-phase translational, rotational, and vibrational contributions to the free energies were determined. The net contribution to the free energy for oxidation amounted to less than 0.01 eV, which is much less than the uncertainty of other approximations in the model. Solvation stabilization energies were estimated by applying the PCM solvation model with dichloromethane as a solvent to the gas phase structures (assuming little change in structure from the gas phase to the condensed phase, as supported by the analysis above).

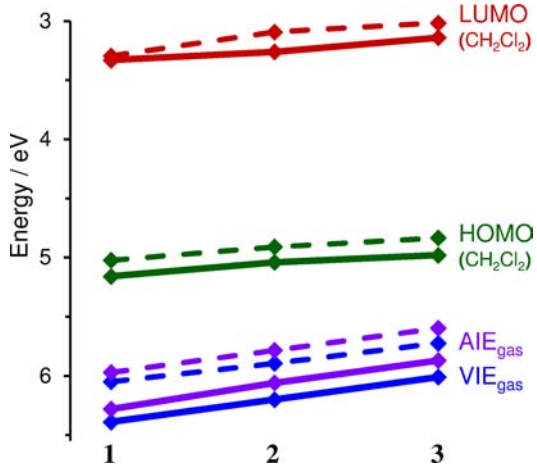

Figure 3. Experimental (solid lines) and computational (dashed lines) energy comparisons for molecules **1**–**3**. VIE and AIE are the gas-phase vertical and adiabatic ionization energies, respectively. HOMO and LUMO are the absolute solution oxidation and reduction potentials, respectively.

The computational energy levels are found to track the experimental values fairly consistently, showing destabilization from molecule **1** to **2** to **3** as discussed previously. The consistency between the calculated and experimental gas-phase energies shown in Figure 3 supports the models for calculation of the electronic energies ΔE. The calculated energy gap between the HOMO and LUMO energies is equal to the experimental value within about 5%. The shift from the gas-phase energies to the solution-phase energies shown in Figure 3 is dominated by the solvation energy, and the similar differences between calculated and experimental energies in both phases indicates that the solvation model and the conversion of the electrochemical potentials to an absolute free energy scale are reasonable.

3.4. Solid Phase. Insight into the intermolecular electronic properties of molecules **1**–**3** is provided by the solid-phase UPS measurements. The solid-phase UPS of TIPS pentacene has been discussed previously[47] in relation to the electronic effect of the triisopropylsilylethynyl group on the pentacene backbone. In this work we focus on the electronic effect of dioxolane functional groups on TIPS pentacene by comparing the electronic properties of TP-5 and EtTP-5 pentacenes with those of TIPS pentacene. Figures 4–6 show the high and low binding energy sides of the photoelectron spectra of pentacenes

dx.doi.org/10.1021/ja3056672 | J. Am. Chem. Soc. 2012, 134, 14185–14194

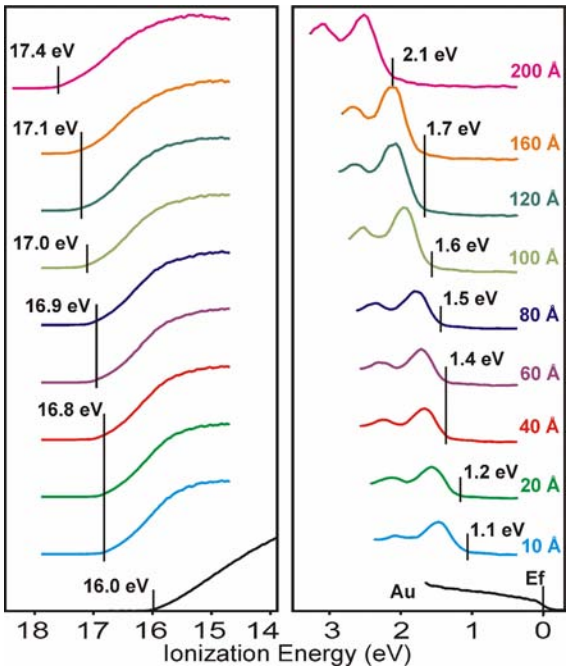

Figure 4. Solid-phase UPS of TIPS pentacene **1** on Au: high binding energy region spectra on the left with HBEC energy indicated, valence region spectra on the right with the ionization onset indicated.

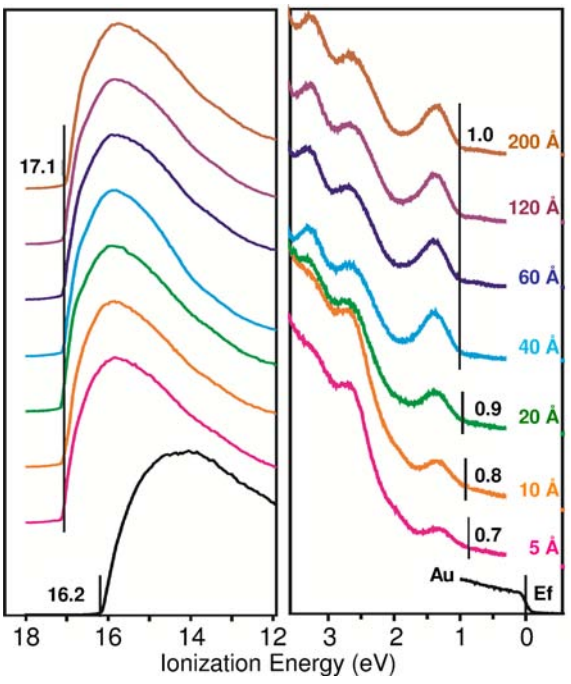

Figure 5. Solid-phase UPS of TP-5 pentacene **2** on Au: high binding energy region spectra on the left with HBEC energy indicated, valence region spectra on the right with the ionization onset indicated.

1−**3** as a function of film thickness. The high binding energy cutoff of ionization intensity (HBEC, which corresponds to the point of electrons with zero kinetic energy from the surface and is used with the photon energy of the source to define the vacuum level of the material) is indicated by the position of the vertical black lines on the left side of the figures. Similarly, the onset of ionization intensity relative to the Fermi level of Au (which corresponds closely to the adiabatic ionization energy

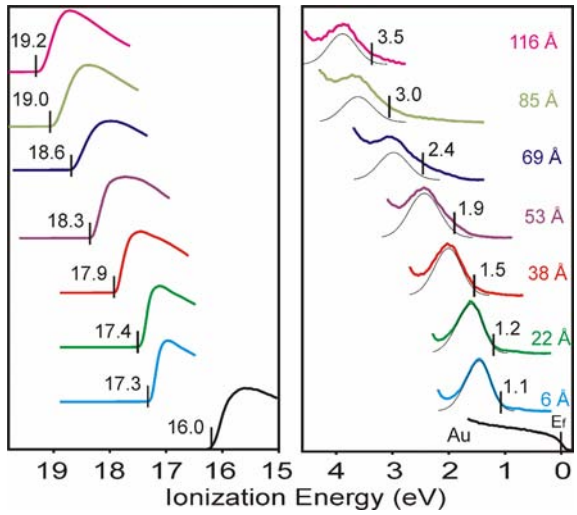

Figure 6. Solid-phase UPS of EtTP-5 pentacene **3** on Au: high binding energy region spectra on the left with HBEC energy indicated, valence region spectra on the right with the ionization onset indicated.: HBEC region spectra on the left, HOMO region spectra on the right.

from the HOMO) is indicated by the vertical black lines on the right side of the figures. The energies of these points are reported to ±0.1 eV. The Fermi level Ef of Au was set to 0.0 eV and the work function of Au for the experiment was the He I photon energy of 21.2 eV minus the HBEC energy.[48]

As can be seen from Figures 4−6, the first deposition of each organic molecule **1**−**3** shifts the HBEC to higher energy on the order of 1 eV from Au. This shift in the vacuum level is caused primarily by the change in the strong surface dipole from the clean gold substrate to the organic surface overlayer.[48−52] In the case of TIPS pentacene **1** (Figure 4), the HBEC continues to shift slowly to higher energy with further depositions up to 160 Å, and a strong shift of HBEC is observed for the 200 Å thick film. This strong HBEC shift for thicknesses above 160 Å indicates insufficient electron transfer through the TIPS pentacene film to compensate charging at the surface. The HOMO AIE level (the top of the valence band) of TIPS pentacene shifts to higher energy slightly more rapidly than the HBEC from the 10 Å film to the 40 Å film due to decreasing stabilization of the TIPS pentacene cation by polarization of the gold substrate.[52] For the films of 40−160 Å, the HOMO and HBEC levels shift similarly (within ±0.1 eV), and for the 200 Å film, the HOMO and HBEC levels shift significantly to higher energy side with the HOMO energy shifting more rapidly due to the charging effects mentioned above. On the basis of these observations, the bulk properties of TIPS pentacene are achieved for the film thicknesses of 100−160 Å because the HBEC and the HOMO level of this material are stabilized within this thickness range.

In the case of TP-5 pentacene **2** (Figure 5), for all depositions from 20 to 200 Å, the HBEC and the HOMO level positions are constant (within the experimental error), meaning that the electron transfer through the TP-5 pentacene film is not affected by the thickness of the film (no charging effects) and the bulk properties are observed for the complete range of thicknesses that were examined.

In contrast, for EtTP-5 pentacene **3** (Figure 6), the HBEC and the HOMO level are never stable. With each increase of film thickness the HBEC and the HOMO level experience strong shifts toward the higher binding energy region, with the

dx.doi.org/10.1021/ja3056672 | J. Am. Chem. Soc. 2012, 134, 14185−14194

HOMO level shifting most rapidly along with a broadening of the peak, indicative of an early onset of charging effects.

On the basis of these results, the evolution of HBEC and HOMO energies with film thickness is strongly affected by the presence of dioxolane-containing substituents on the pentacene backbone, showing different behavior in all three cases. Table 3

Table 3. Experimental Solid-Phase Energy Values in eV of Molecules 1−3

		1	2	3
Zone **A**	range	<60 Å	<60 Å	<60 Å
	AIE_s[a]	≈5.6	≈5.0	≈5.0
	PE[b]	≈0.7	≈1.1	≈0.9
Zone **B**	range	60−160 Å	60−200 Å	—
	AIE_s[a]	5.8	5.1	—
	PE[b]	0.5	1.0	—
Zone **C**	range	≥200 Å	—	>60 Å
	AIE_s[a]	>5.9	—	>5.0
	Δ[c]	<0.4	—	<0.9

[a]Adiabatic ionization energy of the solid (AIE_S) measured relative to the vacuum level = photon energy − HBEC energy + ionization onset energy. [b]Polarization energy (PE) = AIE_G − AIE_S, where AIE_G is the adiabatic ionization energy measured in the gas phase. [c]Shift of the adiabatic ionization energy from the gas phase in the presence of surface charging.

compares the ionization characteristics of thin films of these molecules as a function of the film thickness, and identifies three different zones. Zone **A** corresponds to the initial coverage of the surface for these molecules. This zone is characterized by the initial shift of the vacuum level and relatively rapid shifting of the HBEC and the ionization onset energies. Zone **B** is a region characterized by fairly stable HBEC and adiabatic ionization energies, and is taken to be characteristic of the bulk material removed from the Au substrate interface. The thickness of this zone is different for each molecule. For TIPS pentacene **1**, it ranges from about 40 to 160 Å after which shifting of both the HBEC and the ionization onset is observed; for TP-5 pentacene **2**, the HBEC and HOMO energies are stable from 40 Å to the thickest coverage studied (200 Å), but for EtTP-5 pentacene **3**, there is no region of stable HBEC and HOMO energies that can be characterized as zone **B**. Zone **C** occurs at higher coverage and is characterized by substantial shifts of the HBEC and HOMO to higher energies as a consequence of surface charging and may be accompanied by broadening of the first ionization peak and a less discernible adiabatic ionization onset. The thickness at which this occurs also is different for each molecule. It begins at very low coverage for EtTP-5 pentacene **3**.

These ionization characteristics are evidence that functionalization of TIPS pentacene with the dioxolane rings leads to better electron transfer through TP-5 pentacene films in comparison to that in TIPS pentacene films. However, further functionalization of TP-5 pentacene with ethyl groups on dioxolane rings leads to substantial charging of EtTP-5 pentacene films at low coverage, which is reflected in the strong observed energy shifts of the HOMO and HBEC. Apparently, the presence of the ethyl groups in EtTP-5 pentacene provides additional insulation between the molecules in the solid and, thus, hinders the intermolecular electronic interactions in this material. It is interesting to note that EtTP-5 was found in the gas-phase photoelectron studies to have the lowest sublimation temperature of the three molecules, despite having the highest mass, consistent with the weakest intermolecular interactions for this molecule. Therefore, in EtTP-5 pentacene films the ionized electrons can not be fully replenished from the Au substrate, which leads to the charging effects that are observed. This, in turn, illustrates very poor electron transfer through the EtTP-5 pentacene films, compared to that in TIPS pentacene and TP-5 pentacene films.

Estimation of the polarization energies in these materials provides further clarification of the intermolecular electronic interactions of pentacenes **1**−**3**. In previous works, we demonstrated how the polarization effects can drastically affect the electronic energy levels in molecules of this type, so that they dominate over the intramolecular electronic structure trends on going from pentacene to TIPS pentacene.[47] We also showed the electronic effect of increasing the number of fused rings in TIPS oligoacenes.[53] The present work shows the electronic effects of the dioxolane substituents on the TIPS pentacene core. The polarization energy (PE), as defined in the literature,[54,55] is the difference in the AIE measured in the gas phase (AIE_G) and the AIE measured in the solid phase (AIE_S) relative to the vacuum energy level. The vacuum energy levels in the gas and solid phase experiments are not defined equivalently, but are sufficiently close in these experiments to allow this comparison.[48,52] To be specific, the vacuum level in the gas phase corresponds to an absolute vacuum (free electron with zero kinetic energy at an infinite distance from the system), and the ionization energies are calibrated to the optical threshold ionizations,[56] in this experimental setup the argon $^2P_{3/2}$ ionization. The vacuum level in the solid phase corresponds to the zero kinetic energy of a free electron just outside the solid and inside the instrument, calibrated to the HBEC, where it is still under the influence of the surface dipoles and potentials.[52] Although the definition of the polarization energy mentioned above does not take into account the difference in vacuum energy levels between the gas and solid phases, and therefore adds some uncertainty to the absolute energy values, for these molecular systems, the surface dipoles are similar and small, so the vacuum levels in the solid phase for the different molecules are similar and the energy trends obtained in the gas phase can be compared with the trends measured in the solid phase.

Table 3 includes the polarization energies (PE) for each molecule **1**−**3** in zones **A** and **B**. The polarization energies are on the order of 1 eV or less, and very similar to the solvent stabilization energies discussed in Section 3.3 and shown in Figure 3. The energy shifts in zone **C** are partly due to charging effects and cannot be ascribed solely to polarization energies. The solid phase adiabatic energies relative to the vacuum level as a function of coverage are compared to the adiabatic gas phase ionization energies in Figure 7. As can be seen from Figure 7, the first ionization energy band is shifted to lower ionization energy on going from the gas to the solid phase for all molecules and all film thicknesses. This destabilization occurs because the ground state of the cation is stabilized by the polarization of the surrounding molecules much more than that of the neutral molecule in the solid. This thus leads to the smaller ionization energy in the solid phase versus the gas phase; the amount of this destabilization depends strongly on the material. The arrows indicate the polarization energies that stabilize the cations relative to the neutral molecules in the solid phase and shift the ionizations to lower energies compared to the gas phase. The polarization energy shift for pentacene is

dx.doi.org/10.1021/ja3056672 | J. Am. Chem. Soc. 2012, 134, 14185−14194

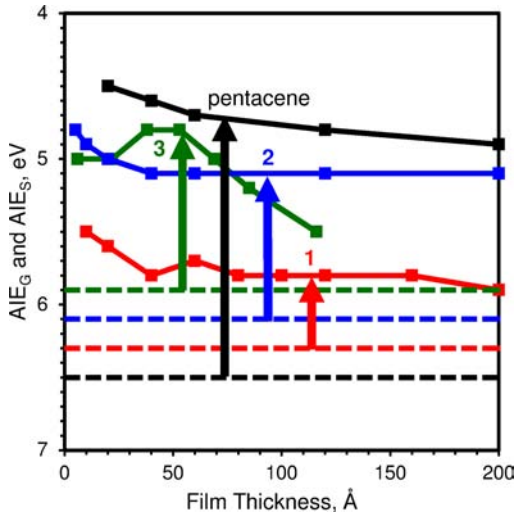

Figure 7. Adiabatic ionization energies measured in the solid phase relative to the vacuum level (AIE_S, solid lines) for pentacene and molecules **1**−**3** as a function of film thickness. The adiabatic ionization energies measured in the gas phase (AIE_G) are shown by the horizontal dashed lines for comparison. The arrows indicate the polarization energies in the solid that stabilize the cations relative to the neutral molecules and shift the ionizations to lower energies.

much larger than that of TIPS pentacene **1**, as discussed in previous work,[47] such that although pentacene has the largest adiabatic ionization energy in the gas phase, it has the lowest adiabatic ionization energy in the solid phase for all film thicknesses. This holds true for pentacene in comparison to TP-5 pentacene **2** and EtTP-5 pentacene **3** also. In the region of 40−60 Å coverage, the solid-state ionization energy trend between TIPS, TP-5, and EtTP-5 pentacenes reproduces the ionization energy trend observed in the gas phase and the oxidation potentials observed in solution; as should be expected, considering similar polarization stabilization of the cations of these molecules with the gold substrate at such low coverages and the weak van der Waals interactions between organic molecules in the solid, which in turn lead to localized HOMO states on each molecule.[57] But going further to the bulk films of pentacenes **1**−**3** (120 Å), the relative shifts in AIE change in different ways. The polarization energy for TIPS pentacene reduces and then stabilizes between 80 and 160 Å. The polarization energy for TP-5 does not reduce as the film thickens, indicating stronger intermolecular interactions, greater polarization energy in the bulk, and less charging. For EtTP-5 pentacene the position of the first energy band shifts consistently to the higher ionization energy for all depositions shortly after the first deposition, thus indicating smaller intermolecular interactions and greater charging. Essentially, the EtTP-5−Au interactions dominate significantly over the EtTP-5−EtTP-5 interactions for thinner layers (up to 50 Å), and when the influence of Au is not observed (70 Å and up), the charging effects start to dominate, indicating overall poor conductivity of EtTP-5 pentacene films. On the basis of these results, TP-5 pentacene films experience the strongest intermolecular electronic interactions in the bulk versus TIPS and EtTP-5 pentacene films. The better conductivity in turn leads to the largest polarization energy and the stable positions of the HBEC and the first energy band without evidence of charging effects.

4. CONCLUSIONS

The results show that (1) the gas-phase ionization energies decrease on going from molecule **1** to **3** due to the addition of oxygen pπ overlap conjugation with acene π orbitals; (2) with these substitutions, the additional vibrations which are activated by ionization lead to a corresponding increase in the intramolecular reorganization energies; (3) in the solution phase, the absolute oxidation potentials are lowered relative to the gas phase fairly uniformly by about 1 eV, primarily by the polarization solvent stabilization of the cations, such that the gas phase trend of lower ionization energy from TIPS to TP-5 to EtTP-5 pentacene is maintained; (4) the reduction potentials of these pentacenes change in parallel with the oxidation potentials, leading to the same energy gap value for TIPS, TP-5, and EtTP-5 pentacenes, because of the similar degree of conjugation in these molecules; (5) the slope of the linear correlation between the solution-phase oxidation potentials and the gas-phase ionization energies is noticeably

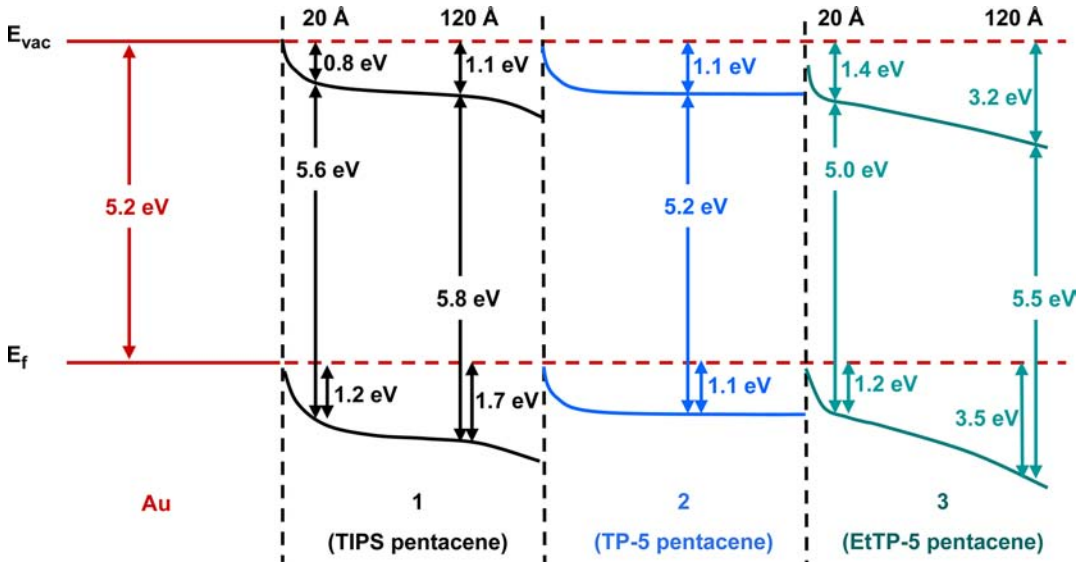

Figure 8. Solid phase energy level diagram of molecules **1**−**3**.

dx.doi.org/10.1021/ja3056672 | J. Am. Chem. Soc. 2012, 134, 14185−14194

smaller than unity meaning that the solvent effects on these pentacenes lead to slower change in oxidation potentials versus the change in ionization energies of molecules **1**−**3**, but the solvent effects are not strong enough to drastically change the oxidation potential trend from the ionization energy trend; (6) in the solid phase for ≈40 Å films, the ionization energy trend of molecules **1**−**3** reproduces the trend observed in the gas phase, because of the similar polarization energies of these materials, whereas for thicker films (∼120 Å), the solid-state ionization energies of pentacenes **1**−**3** do not follow the gas-phase ionization energy trend because of the drastic change in polarization effects observed in the bulk and surface charging of the EtTP-5 films; (7) the intermolecular interactions in TP-5 pentacene films are stronger versus those in TIPS pentacene films; EtTP-5 pentacene films have the weakest intermolecular interactions.

The results of this work are summarized in the solid-state energy level diagram Figure 8. This diagram shows the vacuum level shift from that of Au to pentacenes **1**−**3**, the evolution of the ionization energies relative to the Fermi level Ef and to the vacuum level of Au with the thickness of these organic layers. Originally, TIPS pentacene was functionalized with dioxolane moieties to make TP-5 and EtTP-5 derivatives in order to lower the oxidation and reduction potentials without changing the energy gap; the charge injection properties of TP-5 pentacene (such as charge injection barriers) from Au electrodes were expected to be improved, whereas further modification of dioxolane rings with the ethyl groups to make EtTP-5 pentacene was implemented in order to reduce significantly the intermolecular interactions.[10,20,21] This original goal is fully supported by the results of this study, namely, TP-5 pentacene has smaller ionization energies relative to the Fermi edge of Au (which is defined in the literature[49,52,58−60] as the hole-injection barrier) and to the vacuum energy level, as well as larger polarization energy than TIPS pentacene, meaning that the intermolecular interactions in TP-5 pentacene films are stronger versus those in TIPS pentacene films. The evolution of the ionization and polarization energies with the thickness of EtTP-5 pentacene films, discussed above, serves as evidence of the weaker intermolecular interactions in this material. Also, in solution (as shown above), TP-5 and EtTP-5 derivatives indeed have lower oxidation and reduction potentials versus those of TIPS pentacene, and all three pentacenes have the same energy gap.

Abbreviations. TIPS, triisopropylsilylethynyl; AIE, adiabatic ionization energy; VIE, vertical ionization energy; HBEC, high binding energy cutoff; RE, reorganization energy; PE, polarization energy; HOMO, highest occupied molecular orbital; LUMO, lowest unoccupied molecular orbital; UPS, ultraviolet photoelectron spectroscopy; XPS, X-ray photoelectron spectroscopy

■ ASSOCIATED CONTENT

Ⓢ Supporting Information

The full gas-phase UPS of each molecule, the list of fitting parameters with vibrational fit details used in gas-phase UPS, computational details. This material is available free of charge via the Internet at http://pubs.acs.org.

■ AUTHOR INFORMATION

Corresponding Author

dlichten@email.arizona.edu; lobanova@email.arizona.edu; anthony@uky.edu

Notes

The authors declare no competing financial interest.

■ ACKNOWLEDGMENTS

Support from the National Science Foundation CHE-1041855, CHE-0749530, CHE-1111570 (Arizona) and CHE-0749473 (Kentucky) is gratefully acknowledged.

■ REFERENCES

(1) Lane, P. A.; Palilis, L. C.; Kushto, G. P.; Kafafi, Z. H.; Purushothaman, B.; Anthony, J. E. *Proc. SPIE* **2008**, *7052*, 70521J/1−70521J/6.
(2) Lin, Y.; Gundlach, D. J.; Nelson, S. F.; Jackson, T. N. *IEEE Trans. Electron Devices* **1997**, *44*, 1325−1331.
(3) Palilis, L. C.; Lane, P. A.; Kushto, G. P.; Purushothaman, B.; Anthony, J. E.; Kafafi, Z. H. *Org. Electron.* **2008**, *9*, 747−752.
(4) Park, S. K.; Jackson, T. N.; Anthony, J. E.; Mourey, D. A. *Appl. Phys. Lett.* **2007**, *91*, 063514/1−063514/3.
(5) Payne, M. M.; Parkin, S. R.; Anthony, J. E.; Kuo, C.; Jackson, T. N. *J. Am. Chem. Soc.* **2005**, *127*, 4986−4987.
(6) Platt, A. D.; Day, J.; Subramanian, S.; Anthony, J. E.; Ostroverkhova, O. *J. Phys. Chem. C* **2009**, *113*, 14006−14014.
(7) Sakamoto, Y.; Suzuki, T.; Kobayashi, M.; Gao, Y.; Inoue, Y.; Tokito, S. *Mol. Cryst. Liq. Cryst.* **2006**, *444*, 225−232.
(8) Singh, T. B.; Meghdadi, F.; Guenes, S.; Marjanovic, N.; Horowitz, G.; Lang, P.; Bauer, S.; Sariciftci, N. S. *Adv. Mater. (Weinheim, Ger.)* **2005**, *17*, 2315−2320.
(9) Tang, C. W.; Vanslyke, S. A. *Appl. Phys. Lett.* **1987**, *51*, 913−915.
(10) Wolak, M. A.; Delcamp, J.; Landis, C. A.; Lane, P. A.; Anthony, J. E.; Kafafi, Z. *Adv. Funct. Mater.* **2006**, *16*, 1943−1949.
(11) Kelley, T. W.; Muyres, D. V.; Baude, P. F.; Smith, T. P.; Jones, T. D. *Mater. Res. Soc. Symp. Proc.* **2003**, *771*, 169−179.
(12) Anthony, J. E. *Chem. Rev.* **2006**, *106*, 5028−5048.
(13) Lane, P. A.; Kafafi, Z. H. Solid-State Photovoltaics: A Review of Molecular and Polymeric Devices. In *Organic Photovoltaics: Mechanism, Materials, and Devices*; Sun, S.-S., Sariciftci, N. S,, Eds.; CRC Press: Boca Raton, FL, 2005; Vol. *99*, pp 49−104.
(14) Giri, G.; Verploegen, E.; Mannsfeld, S. C. B.; Atahan-Evrenk, S.; Kim, D. H.; Lee, S. Y.; Becerril, H. A.; Aspuru-Guzik, A.; Toney, M. F.; Bao, Z. *Nature* **2011**, *480*, 504−508.
(15) Han, J.; Bae, I.; Chung, I. *ECS Trans.* **2011**, *33*, 101−111.
(16) Anthony, J. E. In *Functional Organic Materials : Syntheses, Strategies and Applications* ; Mueller, T. J. J.; Bunz, U. H. F., Eds.; Wiley-VCH: Chichester, 2007; *Chapter 4*, pp 511−545.
(17) Anthony, J. E.; Brooks, J. S.; Eaton, D. L.; Parkin, S. R. *J. Am. Chem. Soc.* **2001**, *123*, 9482−9483.
(18) Anthony, J. E.; Purushothaman, B. *Proc. SPIE* **2007**, *6658*, 66580L/1−66580L/8.
(19) Anthony, J. E. *Angew.Chem., Int. Ed.* **2008**, *47*, 452−483.
(20) Wolak, M. A.; Melinger, J. S.; Lane, P. A.; Palilis, L. C.; Landis, C. A.; Delcamp, J.; Anthony, J. E.; Kafafi, Z. H. *J. Phys. Chem. B* **2006**, *110*, 7928−7937.
(21) Wolak, M. A.; Melinger, J. S.; Lane, P. A.; Palilis, L. C.; Landis, C. A.; Anthony, J. E.; Kafafi, Z. H. *J. Phys. Chem. B* **2006**, *110*, 10606−10611.
(22) Siegbahn, K.; Nordling, C.; Fahlman, A.; Nordberg, R.; Hamrin, K.; Hedman, J.; Johansson, G.; Bergmark, T.; Karlsson, S. E.; Lindgren, I.; Lindberg, B. *Nova Acta Regiae Soc. Sci. Ups.* **1967**, *20*, 282.
(23) Lichtenberger, D. L.; Kellogg, G. E.; Kristofzski, J. G.; Page, D.; Turner, S.; Klinger, G.; Lorenzen, J. *Rev. Sci. Instrum.* **1986**, *57*, 2366.
(24) Cranswick, M. A.; Dawson, A.; Cooney, J. J. A.; Gruhn, N. E.; Lichtenberger, D. L.; Enemark, J. H. *Inorg. Chem.* **2007**, *46*, 10639−10646.
(25) Li, Y.; Cao, Y.; Gao, J.; Wang, D.; Yu, G.; Heeger, A. J. *Synth. Met.* **1999**, *99*, 243−248.
(26) de Leeuw, D. M.; Simenon, M. M. J.; Brown, A. R.; Einerhand, R. E. F. *Synth. Met.* **1997**, *87*, 53−59.

(27) Frisch, M. J.; Trucks, G. W.; Schlegel, H. B.; Scuseria, G. E.; Robb, M. A.; Cheeseman, J. R.; Montgomery, J. A., Jr.; Vreven, T.; Kudin, K. N.; Burant, J. C.; Millam, J. M.; Iyengar, S. S.; Tomasi, J.; Barone, V.; Mennucci, B.; Cossi, M.; Scalmani, G.; Rega, N.; Petersson, G. A.; Nakatsuji, H.; Hada, M.; Ehara, M.; Toyota, K.; Fukuda, R.; Hasegawa, J.; Ishida, M.; Nakajima, T.; Honda, Y.; Kitao, O.; Nakai, H.; Klene, M.; Li, X.; Knox, J. E.; Hratchian, H. P.; Cross, J. B.; Bakken, V.; Adamo, C.; Jaramillo, J.; Gomperts, R.; Stratmann, R. E.; Yazyev, O.; Austin, A. J.; Cammi, R.; Pomelli, C.; Ochterski, J. W.; Ayala, P. Y.; Morokuma, K.; Voth, G. A.; Salvador, P.; Dannenberg, J. J.; Zakrzewski, V. G.; Dapprich, S.; Daniels, A. D.; Strain, M. C.; Farkas, O.; Malick, D. K.; Rabuck, A. D.; Raghavachari, K.; Foresman, J. B.; Ortiz, J. V.; Cui, Q.; Baboul, A. G.; Clifford, S.; Cioslowski, J.; Stefanov, B. B.; Liu, G.; Liashenko, A.; Piskorz, P.; Komaromi, I.; Martin, R. L.; Fox, D. J.; Keith, T.; Al-Laham, M. A.; Peng, C. Y.; Nanayakkara, A.; Challacombe, M.; Gill, P. M. W.; Johnson, B.; Chen, W.; Wong, M. W.; Gonzalez, C.; Pople, J. A. *Gaussian 03*; Gaussian, Inc.: Wallingford, CT, 2004. http://www.gaussian.com. See the program documentation on the web site for the definitions and original references to the density functionals, basis sets, and other details of the computational models used in this study.

(28) *ADF2008.01*. SCM, Theoretical Chemistry; Vrije Universiteit: Amsterdam, The Netherlands, 2008; http://www.scm.com. See the program documentation on the web site for the definitions and original references to the density functionals, basis sets, and other details of the computational models used in this study.

(29) *MacroModel*, Version 9.9; Schrödinger, LLC: New York, NY, 2011; http://www.schrodinger.com.

(30) Delgado, M. C. R.; Pigg, K. R.; da Silva Filho, D. A.; Gruhn, N. E.; Sakamoto, Y.; Suzuki, T.; Osuna, R. M.; Casado, J.; Hernández, V.; Navarrete, J. T. L.; Martinelli, N. G.; Cornil, J.; Sánchez-Carrera, R. S.; Coropceanu, V.; Brédas, J. *J. Am. Chem. Soc.* **2009**, *131*, 1502−1512.

(31) Kaur, I.; Jia, W.; Kopreski, R. P.; Selvarasah, S.; Dokmeci, M. R.; Pramanik, C.; McGruer, N. E.; Miller, G. P. *J. Am. Chem. Soc.* **2008**, *130*, 16274−16286.

(32) Coropceanu, V.; Malagoli, M.; da Silva Filho, D. A.; Gruhn, N. E.; Bill, T. G.; Bredas, J. L. *Phys. Rev. Lett.* **2002**, *89*, 275503/1−275503/4.

(33) Griffith, O. L.; Gruhn, N. E.; Anthony, J. E.; Purushothaman, B.; Lichtenberger, D. L. *J. Phys. Chem. C* **2008**, *112*, 20518−20524.

(34) Gruhn, N. E.; da Silva Filho, D. A.; Bill, T. G.; Malagoli, M.; Coropceanu, V.; Kahn, A.; Bredas, J. *J. Am. Chem. Soc.* **2002**, *124*, 7918−7919.

(35) Lichtenberger, D. L.; Copenhaver, A. S. *J. Electron Spectrosc. Relat. Phenom.* **1990**, *50*, 335−352.

(36) Amashukeli, X.; Gruhn, N. E.; Lichtenberger, D. L.; Winkler, J. R.; Gray, H. B. *J. Am. Chem. Soc.* **2004**, *126*, 15566−15571.

(37) Malagoli, M.; Coropceanu, V.; da Silva Filho, D. A.; Bredas, J. L. *J. Chem. Phys.* **2004**, *120*, 7490−7496.

(38) Clark, P. A.; Brogli, F.; Heilbronner, E. *Helv. Chim. Acta* **1972**, *55*, 1415−1428.

(39) Gleiter, R.; Haider, R.; Quast, H. *J. Chem. Res.* **1978**, *4*, 138−139.

(40) Gleiter, R.; Hoffmann, H.; Irngartinger, H.; Nixdorf, M. *Chem. Ber.* **1994**, *127*, 2215−2224.

(41) Gleiter, R.; Uschmann, J. *J. Org. Chem.* **1986**, *51*, 370−380.

(42) Parker, V. D. *J. Am. Chem. Soc.* **1976**, *98*, 98−103.

(43) Vannucci, A. K.; Snyder, R. A.; Gruhn, N. E.; Lichtenberger, D. L.; Enemark, J. H. *Inorg. Chem. (Washington, DC, U. S.)* **2009**, *48*, 8856−8862.

(44) Graff, J. N.; McElhaney, A. E.; Basu, P.; Gruhn, N. E.; Chang, C. J.; Enemark, J. H. *Inorg. Chem.* **2002**, *41*, 2642−2647.

(45) Neikam, W. C.; Dimeler, G. R.; Desmond, M. M. *J. Electrochem. Soc.* **1964**, *111*, 1190−1192.

(46) Matsumura-Inoue, T.; Kuroda, K.; Umezawa, Y.; Achiba, Y. *J. Chem. Soc., Faraday Trans. 2* **1989**, *85*, 857−866.

(47) Griffith, O. L.; Anthony, J. E.; Jones, A. G.; Lichtenberger, D. L. *J. Am. Chem. Soc.* **2010**, *132*, 580−586.

(48) Cahen, D.; Kahn, A. *Adv. Mater.* **2003**, *15*, 271−277.

(49) Amy, F.; Chan, C.; Kahn, A. *Org. Electron.* **2005**, *6*, 85−91.

(50) Kang, S. J.; Yi, Y.; Kim, C. Y.; Cho, S. W.; Noh, M.; Jeong, K.; Whang, C. N. *Synth. Met.* **2006**, *156*, 32−37.

(51) Kahn, A.; Koch, N.; Gao, W. *J. Polym. Sci., Part B: Polym. Phys.* **2003**, *41*, 2529−2548.

(52) Ishii, H.; Sugiyama, K.; Ito, E.; Seki, K. *Adv. Mater.* **1999**, *11*, 605−625.

(53) Griffith, O. L.; Jones, A. G.; Anthony, J. E.; Lichtenberger, D. L. *J. Phys. Chem. C* **2010**, *114*, 13838−13845.

(54) Sato, N.; Seki, K.; Inokuchi, H. *J. Chem. Soc., Faraday Trans. 2* **1981**, *77*, 1621−1633.

(55) Sato, N.; Inokuchi, H.; Silinsh, E. A. *Chem. Phys.* **1987**, *115*, 269−277.

(56) Sansonetti, J. E.; Martin, W. C. *J. Phys. Chem. Ref. Data* **2005**, *34*, 1559−2259.

(57) Bruetting, W., Ed.; In *Physics of Organic Semiconductors*; Wiley-VCH Verlag GmbH & Co. KGaA: Weinheim, Germany, 2005.

(58) Koch, N.; Kahn, A.; Ghijsen, J.; Pireaux, J.; Schwartz, J.; Johnson, R. L.; Elschner, A. *Appl. Phys. Lett.* **2003**, *82*, 70−72.

(59) Schroeder, P. G.; France, C. B.; Park, J. B.; Parkinson, B. A. *J. Phys. Chem. B* **2003**, *107*, 2253−2261.

(60) Mori, T.; Fujikawa, H.; Tokito, S.; Taga, Y. *Appl. Phys. Lett.* **1998**, *73*, 2763−2765.